Intraspinal Delivery of Polyethylene Glycol-coated Gold Nanoparticles Promotes Functional Recovery After Spinal Cord Injury

Florentia Papastefanaki[1], Igor Jakovcevski[2–4], Nafsika Poulia[1], Nevena Djogo[2], Florian Schulz[5], Tamara Martinovic[6], Darko Ciric[6], Gabrielle Loers[2], Tobias Vossmeyer[5], Horst Weller[5,7], Melitta Schachner[8] and Rebecca Matsas[1]

[1]Laboratory of Cellular and Molecular Neurobiology, Hellenic Pasteur Institute, Athens, Greece; [2]Zentrum für Molekulare Neurobiologie, Universitätsklinikum Hamburg-Eppendorf, Universität Hamburg, Hamburg, Germany; [3]Experimental Neurophysiology, University Hospital Cologne, Köln, Germany; [4]Current address: German Center for Neurodegenerative Diseases, Bonn, Germany; [5]Institut für Physikalische Chemie, Universität Hamburg, Hamburg, Germany; [6]Institute of Histology and Embryology, School of Medicine, University of Belgrade, Belgrade, Serbia; [7]Department of Chemistry, Faculty of Science, King Abdulaziz University, Jeddah, Saudi Arabia; [8]Center for Neuroscience, Shantou University Medical College, Guandong, People's Republic of China

Failure of the mammalian central nervous system (CNS) to regenerate effectively after injury leads to mostly irreversible functional impairment. Gold nanoparticles (AuNPs) are promising candidates for drug delivery in combination with tissue-compatible reagents, such as polyethylene glycol (PEG). PEG administration in CNS injury models has received interest for potential therapy, but toxicity and low bioavailability prevents clinical application. Here we show that intraspinal delivery of PEG-functionalized 40-nm-AuNPs at early stages after mouse spinal cord injury is beneficial for recovery. Positive outcome of hind limb motor function was accompanied by attenuated inflammatory response, enhanced motor neuron survival, and increased myelination of spared or regrown/sprouted axons. No adverse effects, such as body weight loss, ill health, or increased mortality were observed. We propose that PEG-AuNPs represent a favorable drug-delivery platform with therapeutic potential that could be further enhanced if PEG-AuNPs are used as carriers of regeneration-promoting molecules.

Received 12 August 2014; accepted 18 March 2015; advance online publication 21 April 2015. doi:10.1038/mt.2015.50

INTRODUCTION

Spinal cord injuries (SCI), affecting mainly young individuals, constitute a serious health problem and functional restoration after SCI remains a significant challenge. SCI results in a primary acute phase followed by secondary damage. Within the first few days after injury, a cascade of deleterious events, including excitotoxicity, oxidative stress, Ca^{2+} influx into cells, inflammation, and cell death, spreads damage from the original site of injury to adjacent tissue. Progression from the acute to the chronic phase results in secondary neurodegenerative events, such as demyelination, Wallerian degeneration, and axonal dieback, while a nonpermissive tissue environment is established largely because of astroglial scar formation, thus contributing to irreversible loss of function.[1–3] A major challenge in SCI repair is to overcome inhibitory cues and enhance those with conducive properties.[3] Several therapeutic interventions have been tested experimentally in animal models of SCI, including administration of anti-inflammatory and neuroprotective factors, regeneration-promoting cell adhesion molecules, microtubule stabilizing agents, enzymes removing glial scar-associated barriers, and blockers of axonal growth inhibitors present in central nervous system (CNS) myelin.[3–8] However, methods of delivery and bioavailability in the host tissue are among the limitations daunting recovery.

Nanoparticles have gained interest as drug delivery systems that could achieve localized and sustained release as well as a favorable risk-to-benefit ratio, important for clinical applications.[9] Thus far, carboxymethylchitosan/polyamidoamine dendrimer nanoparticles,[10] functionalized magnetic iron oxide nanoparticles[11] and poly(lactic-co-glycolic acid) nanoparticles[12] have been investigated in SCI. Alternatively, colloidal gold nanoparticles (AuNPs) appear as leading candidates in the field of nanomedicine, due to their inert and nonimmunogenic characteristics, good biocompatibility and biodistribution, ease of preparation, and modification.[13] Their potential as a versatile platform for drug delivery has been demonstrated in various studies,[14] including targeting of cancer cells. However, less attention has been paid to neurological disorders or neurotrauma. AuNPs can be readily synthesized and functionalized with different biomolecules without alteration of their biological activity.[14–16] Polyethylene glycol (PEG) coating has been applied to increase colloidal stability of AuNPs, enhance their solubility and pharmacokinetic properties, and reduce toxicity.[9,14,17] Nude and PEG-coated AuNPs enter the

I.J. and N.P. contributed equally to this work.

Correspondence: *Rebecca Matsas, Laboratory of Cellular and Molecular Neurobiology, Hellenic Pasteur Institute, 127 Vassilissis Sofias Avenue, 11521 Athens, Greece. E-mail: rmatsa@pasteur.gr or Melitta Schachner, Center for Neuroscience, Shantou University Medical College, 22 Xin Ling Road, Shantou, Guandong 515041, People's Republic of China. E-mail: schachner@stu.edu.cn*

cells by endocytosis-dependent and -independent mechanisms. The type of particle coating influences AuNP cellular entry mechanisms, intracellular trafficking, and tissue penetration.[17]

PEG is a recognized membrane sealant. Due to this property, PEG administration in CNS injury models has been used to promote restoration of function. By decreasing membrane permeability and silencing oxidative stress on neurons and other cell types at the lesion site, PEG reduces inflammation and is neuroprotective.[18–21] Yet, there are limitations to clinically adapting PEG administration emerging mostly from its toxicity and limited bioavailability when given systemically or locally.[22,23] Therefore, recent attempts have focused on optimizing PEG pharmacokinetics by linking it to nanoparticles, such as silica or other nanoscale copolymer micelles.[24–27]

In this study, we present a novel approach for PEG application. PEG was chemically linked to AuNPs and the PEG-functionalized nanoparticles were administered intraspinally acutely after mouse SCI. PEG-AuNPs promoted hind limb motor recovery which was accompanied by attenuated microglial response, enhanced motor neuron protection, and substantially increased remyelination. Our results suggest that PEG-AuNPs can improve recovery after SCI by minimizing the acute phase damage and raise hopes that these beneficial effects may be further augmented when PEG-AuNPs are used as carriers of therapeutic drugs.

RESULTS

Comparison between PEG-functionalized AuNPs and free PEG *in vitro*

We prepared monodentate thiolated polyethylene glycol (PEGMUA; (α-methoxypoly(ethylene glycol)-ω-(11-mercaptoundecanoate) encompassing PEG with a long C10 alkylene spacer)-functionalized AuNPs of 14 and 40 nm particle diameters (PEG-AuNP-14 and PEG-AuNP-40, **Supplementary Figure S1a,b**; **Supplementary information**). The synthesis of this ligand and the superior stability of PEGylated AuNPs with the alkylene spacer has been described.[28] Before proceeding to *in vivo* experiments, we investigated if PEG coupled to AuNP-40 retains its membrane sealing properties, as previously shown for PEG on AuNP-14.[15] To this end, we measured the extent of neurite outgrowth in primary cultures of cerebellar neurons isolated form postnatal day 7 mouse cerebellum that were maintained in the presence of either PEG-AuNP-40 or free PEG. Since during preparation of primary neurons cells undergo injury, their subsequent survival and extension of neurites depends on resealing of damaged membranes. Cerebellar neurons were plated at low density and the length of the newly extended neurite in each cell that had attached to the substrate was estimated after 24 hours in the presence of free PEG, PEG-AuNP-40, or phosphate-buffered saline (PBS) vehicle. We observed enhanced neurite outgrowth in the presence of both PEG and PEG-AuNP-40 as compared to PBS vehicle (**Figure 1a**). In particular, PEG resulted in a 15.5% increase in neurite length as compared to PBS (51.0 ± 2.7 µm for PEG versus 44.2 ± 1.4 µm for PBS, $P = 0.027$) while PEG-AuNP-40 resulted in an 11.1% increase as compared to PBS (49.1 ± 1.7 µm for PEG-AuNP-40 versus 44.2 ± 1.4 µm for PBS, $P = 0.026$) with no significant difference between PEG and PEG-AuNP-40 ($P = 0.563$). The membrane sealing/neuroprotective function of PEG on AuNP-40 was further verified by exposing cerebellar neurons to oxidative stress and measuring cell survival (**Figure 1b**). Twenty-four hours exposure to 10 µmol/l H_2O_2 reduced survival to 38.8 ± 1.4% as compared to nontreated cells (survival 100 ± 1.9%; $P < 0.001$). When cells were exposed H_2O_2 in the presence of PEG, survival was restored to 81.1 ± 2.2% as compared to nontreated cells ($P < 0.001$). Similarly, cotreatment with H_2O_2 and PEG-AuNP-40 restored survival to 89.6 ± 0.9% as compared to nontreated cells ($P < 0.001$). No significant differences were noted between nontreated cells and cells cotreated with H_2O_2 and PEG or PEG-AuNP-40 ($P > 0.05$). These and previous data[15] indicate that PEG retains its membrane sealing/neuroprotective properties when coupled to AuNPs.

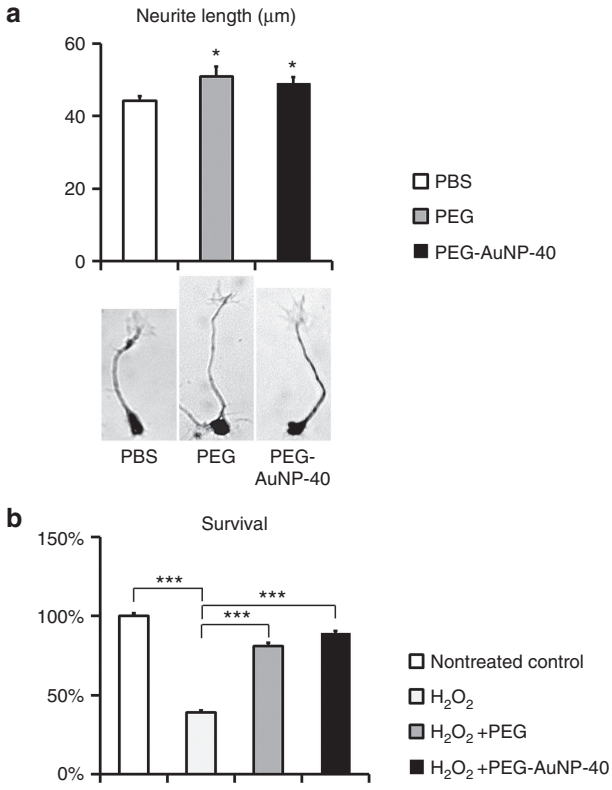

Figure 1 Polyethylene glycol (PEG) on AuNPs is neuroprotective *in vitro*. (**a**) Graph and photomicrographs of representative mouse cerebellar neurons illustrating the extent of neurite outgrowth in cultures maintained in medium containing phosphate-buffered saline (control vehicle), PEG, or PEG-AuNP-40, 24 hours after plating. (**b**) Graph representing % survival of mouse cerebellar neurons after 24 hours exposure to 10 µmol/l H_2O_2 relatively to nontreated control cells, either in the absence or in the presence of free polyethylene glycol PEG and PEG-AuNP-40, respectively. Values represent means ± SEM. $*P \leq 0.05$ and $***P \leq 0.001$ by one-way analysis of variance for overall differences, followed by Holm-Sidak *post hoc* analysis. At least 100 cells were measured (in **a**) in each experimental condition; $n = 12$ samples per treatment in two independent experiments in **b**.

Comparison between PEG-functionalized AuNPs and free PEG *in vivo*

In an initial *in vivo* experiment, we screened the PEG-AuNP-14 and PEG-AuNP-40 particles for their potential to improve the functional outcome after SCI in comparison with free PEG (MW: 2,000; same chain length as PEGMUA on PEG-AuNPs). We used an established

mouse model of spinal cord compression injury[6,29] and acutely delivered the particles via two intraspinal injections, 1 µl each, rostral and caudal to the lesion (**Figure 2a**). Four groups of randomized mice were compared: (i) a PBS control group with five animals (n = 5) receiving two injections of the vehicle; (ii) a PEG group (n = 4) receiving two injections of free PEG2000 solution in PBS; (iii) a PEG-AuNP-14 group (n = 6) receiving two injections of 14-nm PEG-AuNPs at a concentration of 20 nmol/l; (iv) a PEG-AuNP-40 group (n = 6) receiving two injections of 40-nm PEG-AuNPs at a concentration of 2 nmol/l. These concentrations of AuNPs were selected so that similar concentrations of PEG ligands would be presented. Additional control groups receiving either AuNP-14 or AuNP-40 without PEG coating, although desirable, could not be included in the study because uncoated citrate-stabilized AuNPs are incompatible with biological environments, both *in vitro* and *in vivo* due to their high tendency to aggregate and sediment.[15]

General health status was assessed by daily monitoring of body weight during the postoperative period. One week after surgery mice in all groups had lost weight, which was partially recovered during the following weeks. PEG-AuNP-40 and PEG groups recovered their weight more efficiently, as compared to the PBS control and PEG-AuNP-14 groups (**Supplementary Figure S1c**). Statistically significant differences were noted in comparison to the PBS control group only at 7 weeks for the PEG group (4.1 ± 2.8% (P = 0.036)) and from 3 weeks onwards for the PEG-AuNP-40 group (3.1 ± 3.6% reduction of body weight at 7 weeks (P = 0.005)), with the PBS control group showing 15.9 ± 4.0% reduction of body weight at 7 weeks, in comparison to the values

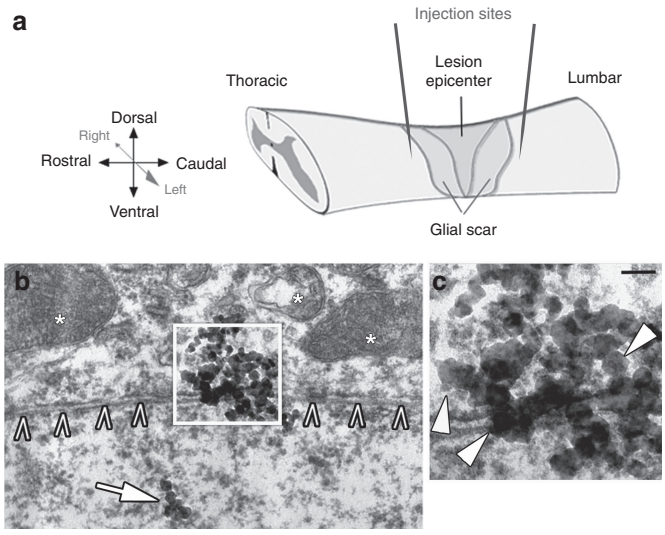

Figure 2 Scheme of experimental outline and documentation of PEG-AuNP-40 in the host tissue by transmission electron microscopy. (**a**) Schematic representation of the mouse spinal cord and histological features appearing after severe spinal cord compression injury (lesion epicenter, glial scar). Red lines indicate the two nanoparticle injection sites located approximately 0.5 mm rostral and caudal to the lesion site. (**b**) 40 nm AuNPs are observed by transmission electron microscopy intracellularly (arrow) and at the level of the plasma membrane of a neuron (carets) 1 week after injury and PEG-AuNP-40 treatment. Intracellular organelles are marked with asterisks; scale bar, 200 nm. (**c**) Higher magnification of the boxed area in **b** where single AuNPs are indicated by arrowheads; scale bar, 100 nm. This figure is available in color in the online version of the article.

before injury. The PEG-AuNP-14 group was indistinguishable from the PBS control group.

To evaluate whether the different treatments could improve motor behavior after injury, all groups were subjected to a set of motor function assays, including the Basso Mouse locomotor rating Scale (BMS), foot-stepping angle, and ladder climbing. Mice were rated before injury, then tested 3 days after injury to examine the extent of paralysis, and subsequently assessed every 2 weeks, for up to 6 weeks. Rating by the BMS score revealed a significant effect at 4 weeks in the PEG-AuNP-40 group as compared with the other groups by two-way analysis of variance for repeated measures, followed by Holm-Sidak *post hoc* analysis (2.8 ± 0.7 for PEG-AuNP-40 group versus 1.5 ± 0.5 for PEG group (P = 0.012); versus 2.0 ± 0.8 for PBS control group (P = 0.043); versus 1.3 ± 0.2 for PEG-AuNP-14 group (P = 0.048)) (**Supplementary Figure S1d**). Notably, the PEG and PEG-AuNP-14 groups behaved similarly to the PBS control group by BMS scoring. Measurement of the foot stepping angle (**Supplementary Figure S1e**) did not reveal any significant effect among the different groups but only a significant effect of time, indicating a similar degree of recovery in all groups. When mice were evaluated with respect to the number of steps performed during climbing the inclined ladder (**Supplementary Figure S1f**), there was a significant effect of time and treatment among groups with *post hoc* analysis revealing at 6 weeks a significant effect of PEG-AuNP-40 versus PEG or PBS treatments (5.8 ± 1.2 correct steps for the PEG-AuNP-40 group versus 1.0 ± 0.7 for the PEG group (P < 0.001) and versus 1.0 ± 0.5 for the PBS control group (P < 0.001)). A significant effect was also noted at 6 weeks postinjury in the PEG-AuNP-14 group versus PEG and PBS control groups (4.2 ± 1.2 correct steps for the PEG-AuNP-14 group versus 1.0 ± 0.7 for the PEG group (P = 0.010) versus 1.0 ± 0.5 for the PBS control group (P = 0.013)). Overall, group comparison analyses of the three behavioral assays and of body weight assessment indicate that (i) free PEG injection does not impede body weight regain but on the other hand is not beneficial for functional recovery; (ii) PEG-AuNP-40 injection does not impede body weight regain and also leads to improved functional recovery (BMS, inclined ladder climbing), and (iii) PEG-AuNP-14 injection interferes with body weight regain and leads to inferior functional recovery as compared to PEG-AuNP-40 (BMS, inclined ladder climbing). The fact that PEG presented on AuNP-14 showed a lower trend for recovery together with its inability to allow efficient body weight gain as compared to PEG on AuNP-40, suggests differences in clearance or retention in tissue, cells and/or the extracellular matrix for the two AuNP sizes. We cannot exclude that differences in toxicity might also play a role.[30]

Analysis of functional recovery after intraspinal delivery of PEG-AuNP-40

Since the results of our initial experiment gave a clear indication in favor of PEG-AuNP-40, we operated a second series of mice to scrutinize PEG-AuNP-40 treatment, this time at a boosted concentration of 5 nmol/l, using detailed motor behavioral and morphological analysis. Two groups of mice received acutely after injury two injections of either PEG-AuNP-40 (n = 6) or PBS vehicle (n = 9), again rostral and caudal to the lesion site and were monitored for 8 weeks after surgery. A PEG group was

not included in the second experimental trial since in the initial experiment it was not different from the PBS control group. The presence of PEG-AuNP-40 particles in the tissue was assured by transmission electron microscopy. One week after injury, electron-dense particles with an approximate 40-nm diameter size were detected throughout the tissue around the lesion site associated with the plasma membrane or localized intracellularly (**Figure 2b,c**).

The first BMS scoring was performed 3 days after injury when all mice showed flaccid hind limb paralysis (**Figure 2a**). Locomotor function was subsequently improved in the PEG-AuNP-40 group to a larger extent as compared to the PBS control group, being significantly different at 2 weeks (P = 0.024), 4 weeks (P = 0.043), and 8 weeks after injury (3.7 ± 0.3 for the PEG-AuNP-40 group versus 1.4 ± 0.5 for the PBS control group, $P < 0.001$, **Figure 3a**). Measurement of foot-stepping angles as an estimate of stepping quality, also revealed a more rapid improvement in the PEG-AuNP-40 group as compared to the PBS control group, with the difference being significant from 2 weeks onwards and considerably enhanced at 8 weeks (77.5° ± 12.9° for the PEG-AuNP-40 group versus 136.4° ± 8.3° for the PBS control group, $P < 0.001$, **Figure 3b**). In the inclined ladder climbing test which provides quantitative evaluation of complex motor behavior demanding precision, the PEG-AuNP-40 group exhibited a trend for better performance than the control PBS group at 4, 6, and 8 weeks after injury, however the effect did not reach statistical significance (P = 0.109, **Figure 3c**). The overall enhanced behavioral outcome of this second experimental set-up on motor function confirmed the beneficial effect of PEG-AuNP-40 when administered intraspinally during the acute phase of injury. The higher concentration of PEG-AuNP-40 used in this second experiment (5 nmol/l) consolidated the differences with stronger significance between the PEG-AuNP-40 and the PBS control group, indicating a dose-dependent effect.

Cellular responses accompanying the enhanced functional recovery

Attenuation of microglial/macrophage response. After compression injury of the spinal cord, a dense fibronectin$^+$ connective tissue matrix fills the lesion site demarcated by a glial fibrillary acidic protein (GFAP)$^+$ area of reactive astrocytes forming the astroglial scar (**Figure 4a**). The intensity of GFAP immunofluorescence quantified in the glial scar adjacent to the lesion site, both rostrally and caudally, showed no difference between the PEG-AuNP-40 and PBS control groups, 8 weeks after injury (**Figure 4b,c** and quantification in d: 1.09 ± 0.09 pixels ($\times 10^7$) in the PBS control group versus 1.18 ± 0.11 in the PEG-AuNP-40 group, P = 0.5534).

Since the immune system reacts to trauma, the microglial/macrophage response to injury[31] was investigated. Resident spinal cord microglia and peripheral macrophages infiltrating the tissue, following disruption of the blood-spinal cord barrier, play a fundamental role in the inflammatory response after injury.[31] Microglial cells adopt an activated phenotype characterized by their amoeboid shape acutely after injury (**Figure 4e** and inset) and persist for several weeks in the tissue playing a dual role: on the one hand, these cells are thought to exert a protective effect, but on the other, especially during the secondary phase of injury, they progressively contribute to tissue degeneration via long-term release of proinflammatory cytokines.[32–34] To assess the effect of PEG-AuNP-40 on microglia/macrophages, immunofluorescence labeling was performed for the marker Iba-1 (ionized calcium-binding adapter molecule 1), 8 weeks after injury (**Figure 4e,f**). Iba-1 staining was reduced in the PEG-AuNP-40 group (**Figure 4f** and inset) as compared to the PBS control group (**Figure 4e** and inset). Of note, the majority of microglial cells in the PEG-AuNP-40 group were of a resting phenotype in contrast to the PBS control group, where many microglia/macrophages exhibited the activated amoeboid shape. Quantification showed that Iba-1 immunofluorescence

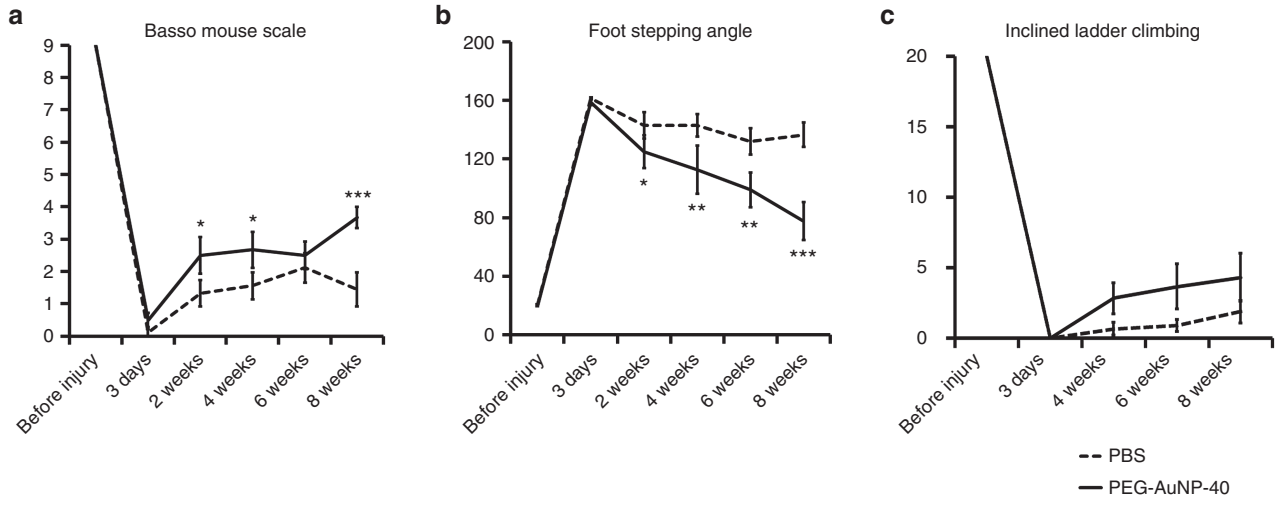

Figure 3 Recovery of hind limb motor function after spinal cord injury in mice treated with PEG-AuNP-40 or phosphate-buffered saline (PBS) vehicle. (**a**) Open-field locomotion scores according to the Basso Mouse Scale (BMS); (**b**) Foot-stepping angles estimated by single-frame motion analysis of beam walking; (**c**) Graph representing the number of correct steps performed on the inclined ladder. Parameters were measured before injury and at the indicated time points after injury. Values represent means ± SEM; $n = 6$ for the PEG-AuNP-40 group and $n = 9$ for the PBS control group; *$P \leq 0.05$, **$P \leq 0.01$, and ***$P \leq 0.001$, by two-way analysis of variance for repeated measures with Holm-Sidak *post hoc* test.

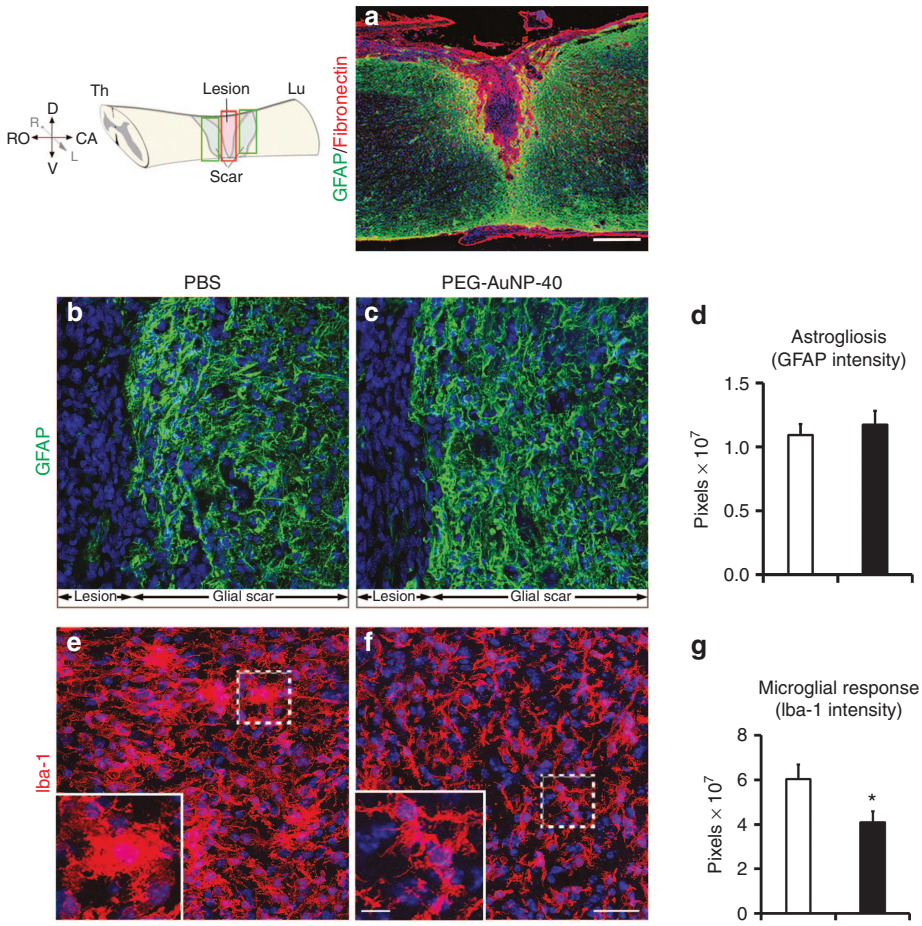

Figure 4 Astroglial and microglial/macrophage reaction in mice treated with PEG-AuNP-40 or phosphate-buffered saline (PBS) vehicle control, 8 weeks after spinal cord injuries. (**a**) Representative image from a parasagittal section of the injured spinal cord after double immunofluorescence staining for the astroglial marker glial fibrillary acidic protein (GFAP) (green) indicating the glial scar and for the meningeal cell marker fibronectin (red) illustrating the lesion epicenter. Nuclei are counterstained with TO-PRO-3 (blue). Scale bar, 250 µm. (**b**,**c**,**e**,**f**) Confocal images with immunofluorescence labeling of parasagittal sections of the lesioned spinal cord from mice of the PBS control group (**b**,**e**) or the PEG-AuNP-40 group (**c**,**f**) stained for GFAP (green; **b**,**c**) or the microglial/macrophage marker Iba-1 (red; **e**,**f**). Images correspond to areas within the lesion site for Iba-1 staining and to areas of the glial scar for glial fibrillary acidic protein (GFAP), as illustrated in the drawing at the top left corner. Boxed areas in **e** and **f** are also shown at higher magnification to highlight the characteristic amoeboid morphology of Iba-1$^+$ cells in the PBS control group indicative of an activated state versus a resting morphology, adopted by many cells in the PEG-AuNP-40 group. Cell nuclei are counterstained with TO-PRO-3 (blue). Scale bar in **f**, 40 µm for **b**, **c**, **e,** and **f**; 10 µm for the insets. (**d**) Quantification of GFAP immunofluorescence revealed no significant difference ($P > 0.05$) between PEG-AuNP-40 group ($n = 6$) and PBS control group ($n = 6$). (**g**) Quantification of Iba-1 immunofluorescence indicates a significant decrease in the PEG-AuNP-40 group ($n = 6$) as compared to the PBS control group ($n = 6$). Values represent means ± SEM. *$P \leq 0.05$, by Student's *t*-test.

intensity in the lesion site was reduced by 32% in the PEG-AuNP-40 group as compared to the PBS control group (pixels (×10^7), 4.1 ± 0.5 for the PEG-AuNP-40 group versus 6.0 ± 0.6 for the PBS control group, $P = 0.0377$; **Figure 4g**). To check whether the decreased Iba-1 immunofluorescence intensity was related to a decrease in the number of Iba1$^+$ cells at the site of injury, we stereologically counted the numerical density of Iba-1$^+$ cells (*i.e.*, the number of cells per unit volume) in approximately 500 µm-long segments of longitudinal spinal cord sections at 250 µm rostral and caudal to the lesion center. Numbers of Iba-1$^+$ cells in the PEG-AuNP-40 group were lower as compared to the PBS control group both rostral or caudal to the lesion site but the difference did not reach statistical significance (averaged densities: 56.3 ± 4.03 cells (×10^3)/mm^3 for the PEG-AuNP-40 group versus 64.9 ± 2.23 cells (×10^3)/mm^3 for the PBS control group, $P = 0.1$).

Protection of motor neurons caudal to the injury site. Given the reported neuroprotective properties of PEG, we investigated if PEG-AuNP-40 treatment could rescue motor neurons in the spinal cord caudal to the lesion site. Transverse sections were immunostained for choline acetyl transferase (ChAT) which is expressed in spinal motor neuronal cell bodies and in cholinergic boutons innervating the motor neurons[29] (**Figure 5a**,**b**,**d**,**e**). A significant 26% increase was observed in the number of motor neurons present in the PEG-AuNP-40 group as compared to the PBS control group (**Figure 5g**; 34 ± 1 motor neurons per section per mouse for the PEG-AuNP-40 group versus 27 ± 1 motor neurons for the PBS control group, $P = 0.0119$). Motor neuron soma size was slightly, but not significantly increased in the PEG-AuNP-40 group when compared to the PBS control group (**Figure 5h**; 952 ± 34 µm^2 for the PEG-AuNP-40 group versus 780 ± 90 µm^2 for the PBS control group, $P = 0.1349$). A small, yet significant, increase of 13%

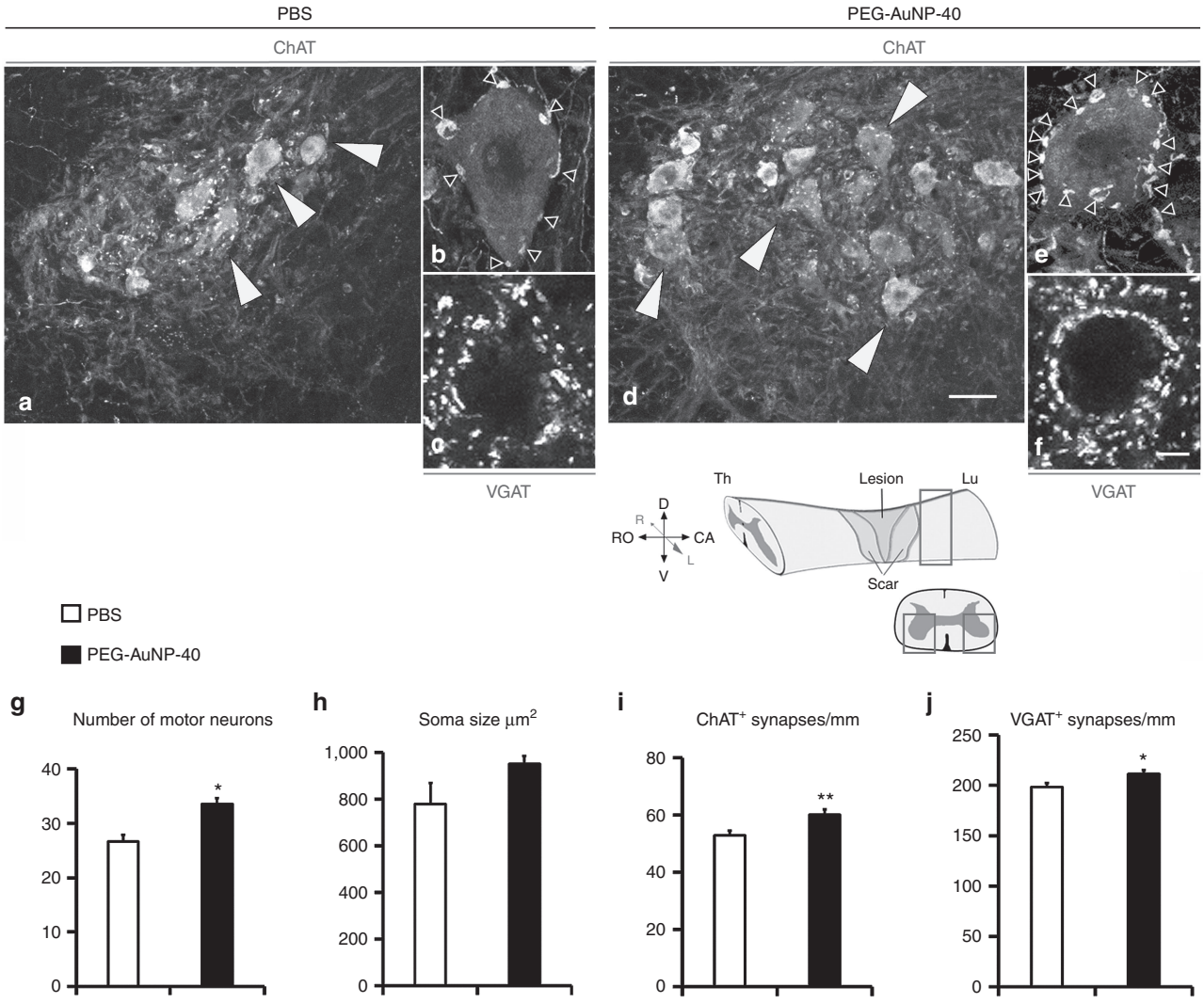

Figure 5 Analysis of motor neurons and perisomatic puncta in the ventral horns of the spinal cord caudal to the lesion site, 8 weeks after spinal cord injuries. (**a–f**) Confocal analysis of spinal cord sections from mice in the phosphate-buffered saline (PBS) control group (**a–c**) or the PEG-AuNP-40 group (**d–f**) immunostained for ChAT (**a**,**b**,**d**,**e**) or VGAT (**c**,**f**). Sections were cut below the lesion site and motor neurons (white arrowheads in **a**,**d**) are visualized in the ventral horns of the spinal cord, as schematized in the accompanying drawing. At higher magnification, ChAT+ (empty arrowheads in **b** and **e**) or VGAT+ immunoreactive puncta (**c**,**f**) are visible around motor neuron cell bodies. TO-PRO-3 counterstain (blue) is seen in **c** and **f**. Scale bar, 40 µm for **a** and **d**, in **d**; 5 µm for **b**,**c**,**e** and **f**, in **f**. **g–j**, Quantification of the number of motor neurons per section per mouse (**g**) and their average soma size in the PEG-AuNP-40 (n = 4 mice) and PBS control group (n = 3 mice) (**h**), as well as the ChAT+ linear perisomatic densities (at least 250 motor neurons were analyzed per group) (**i**) and VGAT+ linear perisomatic densities (150 motor neurons were analyzed per group) (**j**). Soma sizes are not different between groups, but a significant increase is evident in the PEG-AuNP-40 group regarding the numbers of motor neurons and their ChAT+ or VGAT+ perisomatic synaptic puncta. Values represent means ± SEM; *$P \leq 0.05$ and **$P \leq 0.01$ by Student's t-test. This figure is available in color in the online version of the article.

was noted in the linear perisomatic density of ChAT+ synapses on motor neurons of the PEG-AuNP-40 group as compared to the PBS control group (Figure 5i; 60 ± 2 synapses mm^{-1} for the PEG-AuNP-40 group versus 53 ± 2 synapses mm^{-1} for the PBS control group, P = 0.0036). An even smaller, but significant increase of 6.6% was found for the perisomatic densities immunoreactive for the vesicular GABA transporter (VGAT) at inhibitory GABAergic synapses[35] on motor neurons (Figure 5c,f,j; 211 ± 4 synapses mm^{-1} for the PEG-AuNP-40 group versus 198 ± 5 synapses mm^{-1} for the PBS group, P = 0.0297). The above differences in motor neuron cholinergic and GABAergic synaptic inputs become more important in the light of enhanced motor neuron survival in the PEG-AuNP-40 group of mice.

To analyze the levels of spared or regenerating axons in the lesion site, immunofluorescence labeling for neurofilament (NF) protein was performed (Figure 6a–c). Similar numbers of labeled axons were observed in the two groups of mice (49.8 ± 7.3 NF+ fibers per section per mouse in the PBS control group versus 46.2 ± 8.0 in the PEG-AuNP-40, P = 0.748). The numbers of catecholaminergic (TH+; Figure 6d–f) and serotonergic (5-HT+; Figure 6g–i) axons projecting beyond an arbitrarily selected border 250 µm caudal to the lesion site were also determined and similar numbers of immunolabeled fibers were found to cross the border in the two groups of mice (6.0 ± 1.5 TH+ fibers per section per mouse in the PBS control group versus 7.8 ± 3.3 in the PEG-AuNP-40 group, P = 0.627; 3.3 ± 0.9 5-HT+ fibers per section

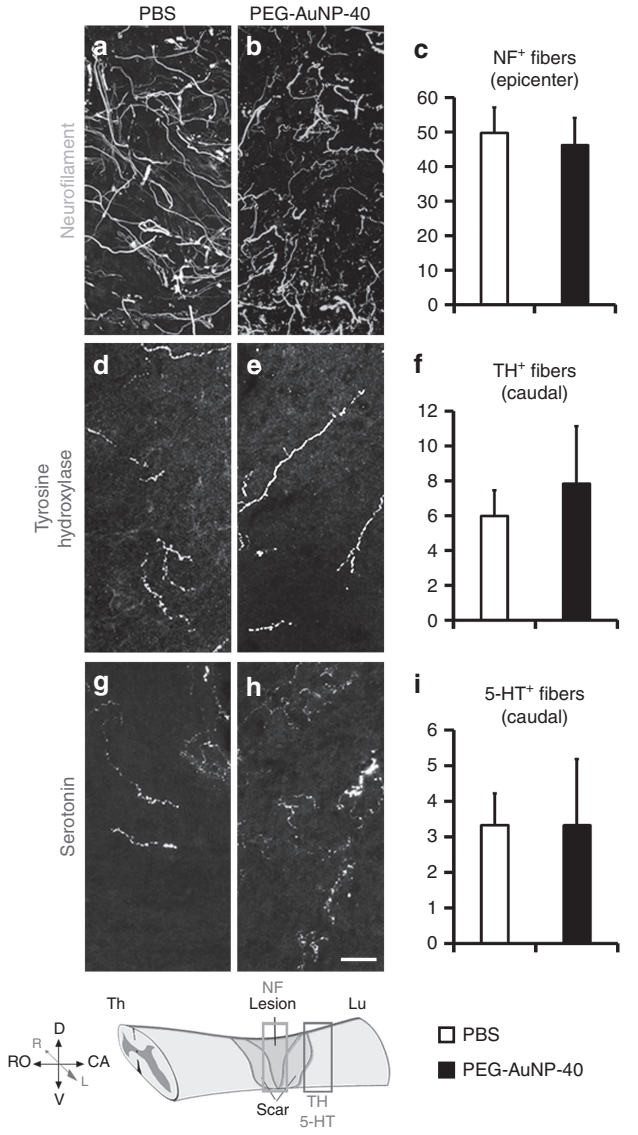

Figure 6 Neuronal fibers in and beyond the lesion site of mice treated with PEG-AuNP-40 or phosphate-buffered saline (PBS) vehicle, 8 weeks after spinal cord injuries. Confocal images of parasagittal sections of injured spinal cords from mice in the PBS control group (**a**,**d**,**g**) or the PEG-AuNP-40 group (**b**,**e**,**h**) immunostained for neurofilament (NF, green, lesion center; **a**,**b**), tyrosine hydroxylase (TH, red, caudal to the lesion site; **d**,**e**) and serotonin (5-HT, red, caudal to the lesion site; **g**,**h**), as shown in the scheme at the bottom left corner. Scale bar, 20 µm. Quantification of the number of neurofilament (NF) positive fibers crossing an arbitrarily positioned line, perpendicularly spanning the lesion site (**c**), number of TH positive fibers (**f**), and 5-HT positive fibers (**i**) crossing an arbitrarily positioned line, perpendicularly spanning the caudal part of the tissue at a distance of 250 µm from the caudal edge of the lesion site, do not show differences between the PBS control and PEG-AuNP-40 groups. $P > 0.05$ by student's *t*-test ($n = 5$ per group for NF, $n = 6$ per group for TH, $n = 3$ per group for 5-HT). Values represent means ± SEM. Statistical analysis was done by Student's *t*-test. This figure is available in color in the online version of the article.

per mouse in the PBS control group versus 3.3 ± 1.8 in the PEG-AuNP-40 group, $P = 1$).

Promotion of remyelination after injury. Demyelination follows after injury of the spinal cord, resulting in disruption of axonal function. Remyelinating oligodendrocytes and Schwann cells are generated after injury from CNS-resident glial progenitors.[36,37] Additionally, Schwann cells from peripheral nerves enter the injured spinal cord through the dorsal root entry zones and contribute to remyelination.[38] However, spontaneous remyelination by oligodendrocytes and Schwann cells[36,37] is insufficient for functional restoration. As an index of remyelination, we evaluated Schwann cell-derived internodal myelin[37] in the injured spinal cord by immunofluorescence staining for the peripheral, but not central, myelin marker P0 protein. As shown in **Figure 7a**,**b**, many P0+ internodal profiles were detected in both groups distributed in the lesioned area and in white matter around the lesion site, yet a marked increase in remyelination was noted in the PEG-AuNP-40 group. Double immunostaining for P0 and contactin associated protein CASPR/paranodin, which is expressed on the axonal cell membrane of myelinated axons at paranodes, indicates proper reconstruction of the newly formed myelin into specialized domains (**Figure 7c**,**d**) essential for axonal function and saltatory propagation of action potential.[39] At 8 weeks after injury, P0 immunofluorescence intensity in and around the lesion site was approximately sevenfolds higher in the PEG-AuNP-40 group as compared to the PBS control group (pixels ($\times 10^7$), 28.2 ± 9.1 for the PEG-AuNP-40 group versus 4.3 ± 0.8 for the PBS control group, $P = 0.0470$; **Figure 7e**).

DISCUSSION

In this study, we showed that intraspinal administration of PEG-functionalized gold nanoparticles during the acute phase after spinal cord injury is beneficial in restoring hind limb motor function. The acceptability of this treatment at present is indicated by the observed health status of the mice, as assessed by body weight regain and inconspicuous morbidity. The positive functional outcome was accompanied in cellular terms by an attenuated microglial/macrophage response, enhanced neuroprotection, and reformation of synapses after injury and increased remyelination.

Regeneration of the adult mammalian CNS is largely prohibited by the hostile tissue environment generated after injury. A microglial/macrophage-based inflammatory response and glial scar formation have been considered to deter regeneration.[3] Axonal regrowth and re-establishment of connections are thus hindered. In our study, we did not gain evidence that improved functional recovery in the PEG-AuNP-40 group of mice could be ascribed to enhanced axonal sparing or regrowth despite the enhanced neurite outgrowth supported by PEG-AuNP-40 in *in vitro*, reflecting the complexity of the environment *in vivo*. Neither did we observe differences in astroglial activation between groups. Nevertheless, our data show considerable increase in motor neuron protection and remyelination by Schwann cells in the PEG-AuNP-40 group, both of which could be causally related to functional restoration. In particular, remyelination restores efficient nerve conduction[40] and it has been argued that reducing conduction block in demyelinated axons which remain viable after SCI represents an important therapeutic target.[41] Previous studies on the therapeutic potential of free PEG or PEG conjugated on nanocarriers in rodent models of spinal cord injury have associated functional recovery with tissue sparing and axonal preservation,[19,24,27] reduced neuroinflammation[24], or increased neuronal survival.[19] On the other hand, our results uniquely underline the importance of myelin sheath

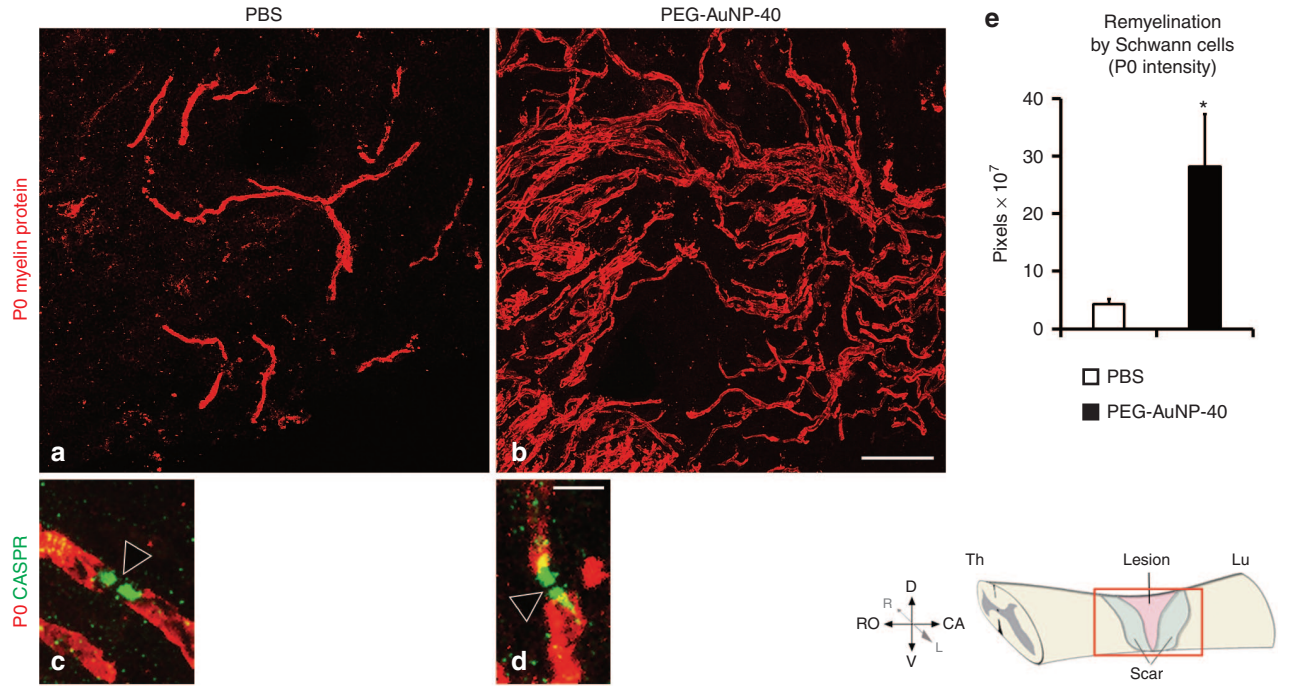

Figure 7 Spontaneous remyelination by Schwann cells is enhanced in mice treated with PEG-AuNP-40, 8 weeks after spinal cord injuries. (**a**,**b**) Immunofluorescence labeling and confocal analysis of parasagittal sections of the lesioned spinal cord from mice of the phosphate-buffered saline (PBS) control group (**a**) or the PEG-AuNP-40 group (**b**) stained for the Schwann cell myelin marker P0 (red). A notable increase in $P0^+$ myelin internodes is apparent in the PEG-AuNP-40 group compared to the PBS group. (**c**,**d**) At high power magnification, double immunofluorescence labeling for P0 (red) and the paranodal marker CASPR/paranodin (green) shows that newly formed myelin paranodal areas (green) are reformed after injury and flank the nodes of Ranvier (empty arrowheads). Scale bar, 40 µm for **a**, **b** in **b**; 5 µm for **c**, **d** in **d**. (**e**) Quantification of total Schwann cell myelin was performed by measuring P0 immunofluorescence intensity showing an increase in the PEG-AuNP-40 group ($n = 6$) as compared to the PBS control group ($n = 6$). $^*P \leq 0.05$, by Student's *t*-test. Values represent means ± SEM.

reformation in functional recovery, presumably by contributing to the restoration of conductivity in spared and/or regrown axons.

Another noteworthy contribution to functional restoration likely depends on significant reduction of the inflammatory response observed in the PEG-AuNP-40 group due to the ability of PEG-AuNPs to protect plasma membranes in the acute phase after injury. As shown by our *in vitro* assays, PEG on AuNPs retains its capacity for restoration of cell membrane integrity and neuroprotection. Healing of damaged membranes should prevent exacerbation of the inflammatory response resulting in increased survival of the different cell populations that exert beneficial functions after injury, including progenitors of myelinating cells. Proinflammatory cytokines such as tumor necrosis factor-α, reactive oxygen species, and toxic levels of nitric oxide released by activated immune cells, are known to cause necrotic or apoptotic death of central nervous system glial cells and glial cell progenitors as well as Schwann cells that invade the lesioned spinal cord.[42–44]

The overall beneficial effects of the PEG-functionalized colloidal gold nanoparticles used in this study are congruent with the membrane-sealing properties of PEG. Due to its ability to restore the integrity of ruptured cell membranes, including those of neurons, glia, and the compromised blood-spinal cord barrier in the injured CNS,[18–21] PEG can be considered to be neuroprotective in a broad spectrum of cellular reactions. For instance, noxious consequences, such as excitotoxic glutamate release,[45] extracellular ATP discharge by astrocytes[46], and fibrinogen leakage by injured endothelial cells[47] are expected to be minimized. In turn, the immune response to injury is likely to be attenuated, thus preventing further tissue damage. Additionally, PEG protects the integrity of mitochondria by reducing Ca^{2+} influx and, consequently, indirectly diminishes the associated detrimental effects of oxidative stress.[20,21]

In this and previous studies, administration of PEGylated nanocarriers was performed acutely after injury.[24,27] However unlike previous reports which apply a subcutaneous[27] or intravenous[24] mode of injection, we have chosen intraspinal delivery aiming to achieve high focal concentration in the lesion site and surrounding tissue while avoiding possible side effects of systemic administration. Growing evidence from clinical studies supports the relevance of immediate intervention after injury. Since early spinal decompression and stabilization surgery, prior to 24 hours after injury, is gaining ground as effective treatment for minimizing neurological damage in patients that are not in a life-threatening situation and without medical comorbidities,[48] a readily available treatment that could be applied at the same time is desirable. Future studies should address the potential of this nanocarrier system as a drug delivery vehicle for acute interventions after injury with the hope that its intrinsic beneficial properties could be combined with biomolecular enhancers of regeneration. Such an approach may also be effective for clinical adaptation not only during the acute, but also the subacute or chronic phases of injury.

MATERIALS AND METHODS

Preparation of PEG-AuNPs. 14-nm (AuNP-14) and 40-nm (AuNP-40) diameter PEG-AuNPs were prepared as previously described.[28] Briefly, PEGMUA (α-methoxypoly(ethylene glycol)-ω-(11-mercaptoundecanoate)) was synthesized by straightforward esterification as described previously.[28,49] AuNPs were synthesized based on a variation of the classical Turkevich method or by the seeded growth synthesis.[50] For PEGylation, 1 mmol/l aqueous PEGMUA solution (assuming MW = 2,000 g mol^{-1}) was mixed with the respective AuNP solutions, and the mixtures were then stirred for 24 hours in a magnetic stirrer. Per AuNP, 6,500 ligands were added in the case of AuNP-14 and 50,000 ligands were added per AuNP in the case of AuNP-40. The PEGylated AuNPs were purified by centrifugation. PEGylated AuNP-14 were centrifuged for 40 minutes at 14,000*g* followed by three centrifugations at 20,000*g* for 15 minutes. PEGylated AuNP-40 were centrifuged for 40 minutes at 2,000*g* followed by three centrifugations at 3,000*g* for 15 minutes. The concentration factors in each centrifugation step were at least 20 and the supernatants were replaced with water, to remove any free ligand. For storage and biological tests, the supernatant in the final centrifugation step was replaced with PBS.

Mouse spinal cord compression injury and intraspinal injections. This study was carried out in strict compliance with the European Directive 2010/63/EU and the Greek National Law 161/91 for Use of Laboratory Animals, according to the Federation of European Laboratory Animal Science Association recommendations for euthanasia and the National Institutes of Health Guide for Care and Use of Laboratory Animals. All protocols were approved by the Institutional Animal Care and Use Committee of the Institutions at the Hamburg-Eppendorf University Medical School and the Hellenic Pasteur Institute (Animal House Establishment Code: EL 25 BIO 013). License No 546/30-01-2013 for the experiments was issued by the Greek authorities of the Veterinary Department of the Athens Prefecture. The manuscript was prepared in compliance with the "Animal Research: Reporting of In Vivo Experiments" guidelines for reporting animal research.

Surgeries were performed as previously described[6,29] in 2- to 3-month-old C57BL/6J female mice anesthetized by intraperitoneal injections of ketamine and xylazine (100 mg of Imalgene 1000 (MERIAL, Lyon, France) and 5 mg Rompun (Bayer, Leverkusen, Germany) kg^{-1} body weight). Laminectomy was performed at the lower thoracic level (T8–T10 vertebrae) with mouse laminectomy forceps. A mouse spinal cord compression device was used for injury consisting of a pair of watchmaker forceps mounted on a metal block attached to a stereotaxic frame. Compression force and duration were controlled by an electromagnetic device. The spinal cord was maximally compressed for 1 second by a time-controlled current flow through the electromagnetic device. The lesion volume was consistent, calculated at $0.53 \pm 0.03\ mm^3$ by reconstruction of consecutive parasagittal sections.

Immediately after compression, lesion animals were randomized into four groups and received two injections of 1 µl PBS vehicle or 2.5% w/v PEG (Sigma, St Louis, MO) solution in PBS or dispersion in PBS of PEG-AuNPs of 14 nm or 40 nm in diameter. The concentrations of AuNPs were selected so that the PEG ligands would be represented at equivalent numbers (approximately 3–4 x 10^{13} PEG ligands in 1 µl dispersion). Injections were performed 0.5 mm rostral and caudal to the lesion site, 1 mm deep into the spinal cord using a stereotactically driven blunt-end Hamilton syringe kept in place for another 2 minutes to avoid backflow. The skin was then sutured using 6-0 nylon stitches. The injury level and injection sites are depicted schematically in **Figure 2a**. After the operation, mice were kept on a heated pad (35–37 °C) overnight to prevent hypothermia and were thereafter singly housed in a temperature-controlled (22 °C) room with water and standard food provided *ad libitum*. During the postoperative period, the bladders of the animals were manually voided twice daily, their general health was closely monitored, and body weight was measured weekly. The numbers of mice per group finally included in each analysis are given in the corresponding fields of the Results section and in figure legends.

Detailed methods for the following tests are presented in Supporting Information: Neurite outgrowth and cell death assays in primary cultures of cerebellar neurons, behavioral assessment of motor function recovery using the Basso Mouse Scale locomotor rating, single-frame motion analysis of foot-stepping angle by beam walking, inclined ladder-climbing test, tissue processing, electron microscopy, immunohistochemistry, estimation of motor neuron soma size and quantification of perisomatic terminals, quantification of spared/regenerating axons, image processing, quantification of fluorescence intensity, stereological analysis and statistical analysis.

SUPPLEMENTARY MATERIAL

Figure S1. Comparison between PEG on AuNPs and free PEG, *in vivo.*
Supplementary Information

ACKNOWLEDGMENTS

This work was supported by the following grants to R.M.: E.U. FP7 REGPOT NEUROSIGN Project 264083, the Hellenic General Secretariat for Research and Technology Grants SYNERGASIA Noiseplus 09SYN-21-969, the Foundation BNP Paribas, Empeirikion Foundation and the framework action KRIPIS to the Hellenic Pasteur Institute co-funded by the European Regional Development Fund and national resources; and to T.V., H.W., G.L., and M.S. by the Landesexzellenzinitiative (LEXI) of Hamburg Nanotechnology in Medicine (NAME). F.P. was recipient of a short-term fellowship from the European Molecular Biology Organization (EMBO, ASTF: 87–2012) and a fellowship from the Theodore-Theochari Cozzika Foundation. We thank Emanuela Szpotowicz at the University of Hamburg for excellent technical assistance. F.P. and I.J. conceived and designed the study, performed the experiments, and analyzed the data; N.P. performed experiments and analyzed the data; F.S., T.V. and H.W. generated and provided AuNPs; N.D. performed experiments and analyzed the data; T.M. and D.C. performed the EM analysis; G.L. contributed to the conception of the hypothesis, performed experiments and contributed materials/analysis tools; M.S. conceived the idea, contributed to implementation and analysis of experiments and provided financial support; R.M. contributed to the study design, interpreted the data, and provided financial support; F.P., M.S., and R.M. wrote the paper. All authors discussed the results and commented on the manuscript.

REFERENCES

1. Schwab, JM, Brechtel, K, Mueller, CA, Failli, V, Kaps, HP, Tuli, SK *et al.* (2006). Experimental strategies to promote spinal cord regeneration–an integrative perspective. *Prog Neurobiol* **78**: 91–116.
2. Oyinbo, CA (2011). Secondary injury mechanisms in traumatic spinal cord injury: a nugget of this multiply cascade. *Acta Neurobiol Exp (Wars)* **71**: 281–299.
3. Thuret, S, Moon, LD and Gage, FH (2006). Therapeutic interventions after spinal cord injury. *Nat Rev Neurosci* **7**: 628–643.
4. Liebscher, T, Schnell, L, Schnell, D, Scholl, J, Schneider, R, Gullo, M *et al.* (2005). Nogo-A antibody improves regeneration and locomotion of spinal cord-injured rats. *Ann Neurol* **58**: 706–719.
5. Lavdas, AA, Papastefanaki, F, Thomaidou, D and Matsas, R (2011). Cell adhesion molecules in gene and cell therapy approaches for nervous system repair. *Curr Gene Ther* **11**: 90–100.
6. Papastefanaki, F, Chen, J, Lavdas, AA, Thomaidou, D, Schachner, M and Matsas, R (2007). Grafts of Schwann cells engineered to express PSA-NCAM promote functional recovery after spinal cord injury. *Brain* **130**(Pt 8): 2159–2174.
7. Hellal, F, Hurtado, A, Ruschel, J, Flynn, KC, Laskowski, CJ, Umlauf, M *et al.* (2011). Microtubule stabilization reduces scarring and causes axon regeneration after spinal cord injury. *Science* **331**: 928–931.
8. Bradbury, EJ, Moon, LD, Popat, RJ, King, VR, Bennett, GS, Patel, PN *et al.* (2002). Chondroitinase ABC promotes functional recovery after spinal cord injury. *Nature* **416**: 636–640.
9. Lipka, J, Semmler-Behnke, M, Sperling, RA, Wenk, A, Takenaka, S, Schleh, C *et al.* (2010). Biodistribution of PEG-modified gold nanoparticles following intratracheal instillation and intravenous injection. *Biomaterials* **31**: 6574–6581.
10. Cerqueira, SR, Oliveira, JM, Silva, NA, Leite-Almeida, H, Ribeiro-Samy, S, Almeida, A *et al.* (2013). Microglia response and *in vivo* therapeutic potential of methylprednisolone-loaded dendrimer nanoparticles in spinal cord injury. *Small* **9**: 738–749.
11. Sharma, HS, Menon, PK, Lafuente, JV, Aguilar, ZP, Wang, YA, Muresanu, DF *et al.* (2014). The role of functionalized magnetic iron oxide nanoparticles in the central nervous system injury and repair: new potentials for neuroprotection with Cerebrolysin therapy. *J Nanosci Nanotechnol* **14**: 577–595.
12. Ren, H, Han, M, Zhou, J, Zheng, ZF, Lu, P, Wang, JJ *et al.* (2014). Repair of spinal cord injury by inhibition of astrocyte growth and inflammatory factor synthesis through local delivery of flavopiridol in PLGA nanoparticles. *Biomaterials* **35**: 6585–6594.

13. Boisselier, E and Astruc, D (2009). Gold nanoparticles in nanomedicine: preparations, imaging, diagnostics, therapies and toxicity. *Chem Soc Rev* **38**: 1759–1782.
14. Khlebtsov, N and Dykman, L (2011). Biodistribution and toxicity of engineered gold nanoparticles: a review of *in vitro* and *in vivo* studies. *Chem Soc Rev* **40**: 1647–1671.
15. Schulz, F, Lutz, D, Rusche, N, Bastús, NG, Stieben, M, Höltig, M *et al.* (2013). Gold nanoparticles functionalized with a fragment of the neural cell adhesion molecule L1 stimulate L1-mediated functions. *Nanoscale* **5**: 10605–10617.
16. Algar, WR, Prasuhn, DE, Stewart, MH, Jennings, TL, Blanco-Canosa, JB, Dawson, PE *et al.* (2011). The controlled display of biomolecules on nanoparticles: a challenge suited to bioorthogonal chemistry. *Bioconjug Chem* **22**: 825–858.
17. Brandenberger, C, Mühlfeld, C, Ali, Z, Lenz, AG, Schmid, O, Parak, WJ *et al.* (2010). Quantitative evaluation of cellular uptake and trafficking of plain and polyethylene glycol-coated gold nanoparticles. *Small* **6**: 1669–1678.
18. Luo, J, Borgens, R and Shi, R (2002). Polyethylene glycol immediately repairs neuronal membranes and inhibits free radical production after acute spinal cord injury. *J Neurochem* **83**: 471–480.
19. Baptiste, DC, Austin, JW, Zhao, W, Nahirny, A, Sugita, S and Fehlings, MG (2009). Systemic polyethylene glycol promotes neurological recovery and tissue sparing in rats after cervical spinal cord injury. *J Neuropathol Exp Neurol* **68**: 661–676.
20. Luo, J, Borgens, R and Shi, R (2004). Polyethylene glycol improves function and reduces oxidative stress in synaptosomal preparations following spinal cord injury. *J Neurotrauma* **21**: 994–1007.
21. Luo, J and Shi, R (2004). Diffusive oxidative stress following acute spinal cord injury in guinea pigs and its inhibition by polyethylene glycol. *Neurosci Lett* **359**: 167–170.
22. Cho, Y and Borgens, RB (2012). Polymer and nano-technology applications for repair and reconstruction of the central nervous system. *Exp Neurol* **233**: 126–144.
23. Cole, A and Shi, R (2005). Prolonged focal application of polyethylene glycol induces conduction block in guinea pig spinal cord white matter. *Toxicol In Vitro* **19**: 215–220.
24. Shi, Y, Kim, S, Huff, TB, Borgens, RB, Park, K, Shi, R *et al.* (2010). Effective repair of traumatically injured spinal cord by nanoscale block copolymer micelles. *Nat Nanotechnol* **5**: 80–87.
25. Chen, B, Zuberi, M, Borgens, RB and Cho, Y (2012). Affinity for, and localization of, PEG-functionalized silica nanoparticles to sites of damage in an ex vivo spinal cord injury model. *J Biol Eng* **6**: 18.
26. Cho, Y, Shi, R, Borgens, R and Ivanisevic, A (2008). Repairing the damaged spinal cord and brain with nanomedicine. *Small* **4**: 1676–1681.
27. Cho, Y, Shi, R, Ivanisevic, A and Borgens, RB (2010). Functional silica nanoparticle-mediated neuronal membrane sealing following traumatic spinal cord injury. *J Neurosci Res* **88**: 1433–1444.
28. Schulz, F, Vossmeyer, T, Bastús, NG and Weller, H (2013). Effect of the spacer structure on the stability of gold nanoparticles functionalized with monodentate thiolated poly(ethylene glycol) ligands. *Langmuir* **29**: 9897–9908.
29. Apostolova, I, Irintchev, A and Schachner, M (2006). Tenascin-R restricts posttraumatic remodeling of motoneuron innervation and functional recovery after spinal cord injury in adult mice. *J Neurosci* **26**: 7849–7859.
30. Cho, WS, Cho, M, Jeong, J, Choi, M, Cho, HY, Han, BS *et al.* (2009). Acute toxicity and pharmacokinetics of 13 nm-sized PEG-coated gold nanoparticles. *Toxicol Appl Pharmacol* **236**: 16–24.
31. David, S and Kroner, A (2011). Repertoire of microglial and macrophage responses after spinal cord injury. *Nat Rev Neurosci* **12**: 388–399.
32. Beck, KD, Nguyen, HX, Galvan, MD, Salazar, DL, Woodruff, TM and Anderson, AJ (2010). Quantitative analysis of cellular inflammation after traumatic spinal cord injury: evidence for a multiphasic inflammatory response in the acute to chronic environment. *Brain* **133**(Pt 2): 433–447.
33. Kigerl, KA, Gensel, JC, Ankeny, DP, Alexander, JK, Donnelly, DJ and Popovich, PG (2009). Identification of two distinct macrophage subsets with divergent effects causing either neurotoxicity or regeneration in the injured mouse spinal cord. *J Neurosci* **29**: 13435–13444.
34. Yang, L, Jones, NR, Blumbergs, PC, Van Den Heuvel, C, Moore, EJ, Manavis, J *et al.* (2005). Severity-dependent expression of pro-inflammatory cytokines in traumatic spinal cord injury in the rat. *J Clin Neurosci* **12**: 276–284.
35. Nikonenko, AG, Sun, M, Lepsveridze, E, Apostolova, I, Petrova, I, Irintchev, A *et al.* (2006). Enhanced perisomatic inhibition and impaired long-term potentiation in the CA1 region of juvenile CHL1-deficient mice. *Eur J Neurosci* **23**: 1839–1852.
36. Zawadzka, M, Rivers, LE, Fancy, SP, Zhao, C, Tripathi, R, Jamen, F *et al.* (2010). CNS-resident glial progenitor/stem cells produce Schwann cells as well as oligodendrocytes during repair of CNS demyelination. *Cell Stem Cell* **6**: 578–590.
37. Powers, BE, Sellers, DL, Lovelett, EA, Cheung, W, Aalami, SP, Zapertov, N *et al.* (2013). Remyelination reporter reveals prolonged refinement of spontaneously regenerated myelin. *Proc Natl Acad Sci USA* **110**: 4075–4080.
38. Brook, GA, Plate, D, Franzen, R, Martin, D, Moonen, G, Schoenen, J *et al.* (1998). Spontaneous longitudinally orientated axonal regeneration is associated with the Schwann cell framework within the lesion site following spinal cord compression injury of the rat. *J Neurosci Res* **53**: 51–65.
39. Poliak, S and Peles, E (2003). The local differentiation of myelinated axons at nodes of Ranvier. *Nat Rev Neurosci* **4**: 968–980.
40. Smith, KJ, Blakemore, WF and McDonald, WI (1981). The restoration of conduction by central remyelination. *Brain* **104**: 383–404.
41. James, ND, Bartus, K, Grist, J, Bennett, DL, McMahon, SB and Bradbury, EJ (2011). Conduction failure following spinal cord injury: functional and anatomical changes from acute to chronic stages. *J Neurosci* **31**: 18543–18555.
42. Boyle, K, Azari, MF, Cheema, SS and Petratos, S (2005). TNFalpha mediates Schwann cell death by upregulating p75NTR expression without sustained activation of NFkappaB. *Neurobiol Dis* **20**: 412–427.
43. Trivedi, A, Olivas, AD and Noble-Haeusslein, LJ (2006). Inflammation and Spinal Cord Injury: Infiltrating Leukocytes as Determinants of Injury and Repair Processes. *Clin Neurosci Res* **6**: 283–292.
44. Wu, J, Yoo, S, Wilcock, D, Lytle, JM, Leung, PY, Colton, CA *et al.* (2010). Interaction of NG2(+) glial progenitors and microglia/macrophages from the injured spinal cord. *Glia* **58**: 410–422.
45. Taylor, DL, Jones, F, Kubota, ES and Pocock, JM (2005). Stimulation of microglial metabotropic glutamate receptor mGlu2 triggers tumor necrosis factor alpha-induced neurotoxicity in concert with microglial-derived Fas ligand. *J Neurosci* **25**: 2952–2964.
46. Davalos, D, Grutzendler, J, Yang, G, Kim, JV, Zuo, Y, Jung, S *et al.* (2005). ATP mediates rapid microglial response to local brain injury in vivo. *Nat Neurosci* **8**: 752–758.
47. Davalos, D, Ryu, JK, Merlini, M, Baeten, KM, Le Moan, N, Petersen, MA *et al.* (2012). Fibrinogen-induced perivascular microglial clustering is required for the development of axonal damage in neuroinflammation. *Nat Commun* **3**: 1227.
48. Fehlings, MG, Vaccaro, A, Wilson, JR, Singh, A, W Cadotte, D, Harrop, JS *et al.* (2012). Early versus delayed decompression for traumatic cervical spinal cord injury: results of the Surgical Timing in Acute Spinal Cord Injury Study (STASCIS). *PLoS One* **7**: e32037.
49. Thiry, M, Boldt, K, Nikolic, MS, Schulz, F, Ijeh, M, Panicker, A *et al.* (2011). Fluorescence properties of hydrophilic semiconductor nanoparticles with tridentate polyethylene oxide ligands. *ACS Nano* **5**: 4965–4973.
50. Bastús, NG, Comenge, J and Puntes, V (2011). Kinetically controlled seeded growth synthesis of citrate-stabilized gold nanoparticles of up to 200 nm: size focusing versus Ostwald ripening. *Langmuir* **27**: 11098–11105.